HHS Public Access

Author manuscript

Clin Imaging. Author manuscript; available in PMC 2024 October 01.

Published in final edited form as:

Clin Imaging. 2023 October ; 102: 109–115. doi:10.1016/j.clinimag.2023.08.004.

Virtual Monoenergetic Imaging in Photon-Counting CT of the Head and Neck

Faraz Farhadi, BS[a], **Pooyan Sahbaee, PhD**[b], **Jayasai R. Rajagopal, BA**[a,c], **Moozhan Nikpanah, MD**[a], **Babak Saboury, MD, MPH**[a], **Ralf Gutjahr, PhD**[d], **Nadia M. Biassou, MD, PhD**[a], **Ritu Shah, MD**[a], **Thomas G. Flohr, PhD**[d], **Ehsan Samei, PhD**[c], **William F. Pritchard, MD, PhD**[a,e], **Ashkan A. Malayeri, MD**[a], **David A. Bluemke, MD, PhD**[f], **Elizabeth C. Jones, MD**[a]

[a.]Radiology and Imaging Sciences, Clinical Center, National Institutes of Health, Bethesda, MD, USA

[b.]Siemens Medical Solutions USA, Malvern, PA, USA

[c.]Carl E. Ravin Advanced Imaging Laboratories, Department of Radiology, Duke University Medical Center, Durham, NC, USA

[d.]Siemens Healthineers, Forchheim, Germany

[e.]Center for Interventional Oncology, Radiology and Imaging Sciences, Clinical Center, National Institutes of Health, Bethesda, MD, USA

[f.]Department of Radiology, University of Wisconsin, Madison, WI, USA

Abstract

Purpose: Advantages of virtual monoenergetic images (VMI) have been reported for dual energy CT of the head and neck, and more recently VMIs derived from photon-counting (PCCT) angiography of the head and neck. We report image quality metrics of VMI in a PCCT angiography dataset, expanding the anatomical regions evaluated and extending observer-based qualitative methods further than previously reported.

Methods: In a prospective study, asymptomatic subjects underwent contrast enhanced PCCT of the head and neck using an investigational scanner. Image sets of low, high, and full spectrum (Threshold-1) energies; linear mix of low and high energies (Mix); and 23 VMIs (40–150keV, 5keV increments) were generated. In 8 anatomical locations, SNR and radiologists' preferences for VMI energy levels were measured using a forced-choice rank method (4 observers) and ratings

Corresponding author: Elizabeth C. Jones, M.D., M.P.H., M.B.A. Radiology and Imaging Sciences, Clinical Center National Institutes of Health, 10 Center Drive, Room 1C355, MSC 1182 Bethesda, MD 20892, Tel: (301) 402-5606. ejones@cc.nih.gov.

of image quality using visual grading characteristic (VGC) analysis (2 observers) comparing VMI to Mix and Threshold-1 images.

Results: Fifteen subjects were included (7 men, 8 women, mean 57 years, range 46–75). Among all VMIs, SNRs varied by anatomic location. The highest SNRs were observed in VMIs. Radiologists preferred 50–60keV VMIs for vascular structures and 75–85keV for all other structures. Cumulative ratings of image quality averaged across all locations were higher for VMIs with areas under the curve of VMI vs Mix and VMI vs Threshold-1 of 0.67 and 0.68 for the first reader and 0.72 and 0.76 for the second, respectively.

Conclusion: Preferred keV level and quality ratings of VMI compared to mixed and Threshold-1 images varied by anatomical location

Keywords

Photon counting CT; Virtual monoenergetic imaging; Head and neck CT; Visual grading characteristic

Introduction:

Methods for dual energy CT (DECT), a subset of spectral CT imaging using two energy levels, were proposed by Hounsfield in 1973 and Alvarez and Macovski in 1976 [1, 2]. Various technical approaches to perform DECT were subsequently developed by major manufacturers, and widespread clinical application began in the 2000's. Clinical applications of spectral imaging with DECT have focused on material decomposition and methods to post-process and display DECT images for clinical interpretation. Full utilization of DECT in practice appears contingent upon acceptable workflow solutions that facilitate clinical review of DECT data.

A single display that takes advantage of information in both low and higher energy acquisitions was desirable for clinical interpretation of DECT but required the development and refinement of processing methods to reduce noise in selective energy data sets [3]. These methods were applied to improve upon blended images and virtual monoenergetic images (VMI) generated from DECT data for clinical applications [4, 5].

Recently, photon-counting detectors (PCD) capable of resolving the high photon flux from clinical CT scans have been developed, described in recent reviews [6, 7]. Due to their construction, these detector systems can reduce noise, increase resolution, and by default collect spectral data which can be separated into 2 or more bins according to energy level by varying the pulse height discrimination as a component of the application-specific integrated circuit [8]. Spectral imaging acquisition with two energy windows can be combined as full spectral data or processed as dual energy imaging data to generate blended and/or VMI images.

Early studies of photon-counting CT (PCCT) using an investigational scanner have compared the performance of full spectral images from PCD with those of conventional energy integrating detectors (EID) [9–13]. Studies using later versions of an investigational PCCT [14] and the product PCCT scanner NAEOTOM Alpha (Siemens) [15, 16] have

confirmed clinical image equivalence and applied post-processing techniques to the data such as VMI for CT of the chest and abdomen. CT angiography of the aorta, virtual non-contrast images of the liver [16] and calcium removal [17].

In October 2021 the Food and Drug Administration cleared the first commercial PCCT scanner in the United States [18]. The clinical photon counting scanner has been released in Europe and the U.S. with routine VMI reconstruction for the diagnostic imaging workflow introduced by the vendor. The image quality of CT using the new scanner has been assessed using traditional physics metrics [19] and with traditional reader studies of image quality. The clinical value of this technology will depend on dose which may be able to be lowered compared to conventional EID CT and image diagnostic quality. In this study, we described image quality of VMIs generated from contrast enhanced PCCT of the head and neck, determined observers' preference for energy levels of VMI by anatomic area or tissue, and compared image quality ratings of optimal VMI to full spectral and blended images.

Methods:

Research subjects

The analysis was performed on data from a prospective study conducted under a protocol approved by the Institutional Review Board. Between December of 2015 and February of 2017, fifteen asymptomatic subjects older than 45 years were enrolled. Written informed consent was obtained from each research participant prior to enrollment in this protocol (NCT02242448). Exclusion criteria included age less than 18 years, pregnancy or breastfeeding, renal insufficiency, allergy to iodinated contrast, known or suspected genetic predisposition to cancer, prior CT in the past year, use of metformin within the prior 24 hours, or inability to undergo CT due to weight, size, or claustrophobia.

Image acquisition and reconstruction: Investigational PCCT System

Imaging studies were performed using an investigational whole-body photon-counting CT scanner (SOMATOM CounT, Siemens Healthineers, Forchheim, Germany), which was based upon a modified dual-source dual-energy scanner (SOMATOM Definition Flash, Siemens Healthineers). The scanner was comprised of a subsystem with an EID and a subsystem with a CdTe PCD [20]. Participants in this clinical study underwent imaging with both subsystems. A prior report compared EID versus PCD image quality using this patient cohort [13]. The current report evaluates optimal parameters for PCD images for VMI and blended images in a reader analysis study of the head and neck.

PCCT images were acquired using a 64×0.5mm collimation at 140 kVp and 108 mAs with two energy thresholds, a lower one at 25 keV which excluded electronic noise and one at 75 keV, separating detector signal into 2 bins of low (<75 keV) and high (>75 keV) energy photons. Subjects were scanned in the supine position, in a craniocaudal acquisition extending from the cranial vertex to the suprasternal notch. Iodinated contrast material (iopamidol, 370 mg I/mL, Isovue-370, Bracco Diagnostics, Melville, NY) at a dose of 1 mL/kg body weight up to a maximum of 105 mL was injected intravenously at rate of 3.0 mL/sec followed by a 20-mL saline bolus at the same flow rate.

Three image sets of low (25–75 keV: Bin1), high (75–140 keV: Bin2), and full spectrum (25–140 keV: Threshold-1) were generated. Images were reconstructed using weighted filtered back projection (ReconCT version 1.3.1.45000; Siemens Healthineers) at a 1.5 mm section thickness and 1.5 mm increment using the medium smooth D30 kernel. Binned datasets generated linear blended (0.6 Bin1:0.4 Bin2 ratio; Mix) and virtual monoenergetic (40–150 keV, at 5 keV increments) (Mono+, Siemens Healthineers) image series. All reconstructions were performed with a field of view of 275 mm and a 512×512 matrix. Image reconstruction and post-processing resulted in 27-image series for each subject: Bin1, Bin2, Threshold-1, Mix, and 23 VMIs.

Quantitative Image Analysis

All image sets were exported from PACS in DICOM format and analyzed using MATLAB (2019b, MathWorks, Natick, MA). Regions of interest (ROI) were placed in eight anatomical locations: common carotid artery, internal jugular vein, cisterna magna, white matter in the frontal lobes, thalamus, pons, midbrain, and medulla oblongata. ROIs were repeated across all image series. The mean value in Hounsfield units, μ_{ROI}, within each ROI represented signal and the standard deviation, σ_{ROI}, represented noise. Signal-to-noise ratio (SNR) was calculated by

$$SNR_{ROI} = \mu_{ROI}/\sigma_{ROI}$$

Observer-based Image Quality Assessment

Qualitative image analysis was performed with two observer studies. In the first observer study, image quality of VMIs at different energy levels were compared in each anatomical structure to determine the preferred VMI level, defined as the level with the highest agreement among all readers. In the second study, images at the preferred VMI level were compared to Mix and Threshold-1 PCCT images at each anatomic location. Observer studies were performed on a system with a DICOM-calibrated medical-grade liquid-crystal display in a reading environment with ambient light less than 5 lumens. Images were presented with fixed standard soft tissue window width/window level of 500/120 for carotid, 350/100 for jugular, and 75/50 for all other locations.

The first observer study used a 10-alternative forced choice design to compare VMIs of different energies. Observers were presented with 10 images from 45–90 keV at 5 keV increments for each patient and were asked to identify three most preferred images for each structure. Readers deemed VMIs greater than 90 keV were of lower quality and were not included in the analysis. The 10 images were viewed in a single panel with order of presentation randomized. Each observer completed 120 assessments across each of eight anatomical locations in 15 subjects, reviewing a total of 1,200 images. Four observers (two neuroradiologists and two body radiologists (14, 15, 8, and 14 years of experience, respectively) blinded to the VMI energy levels participated in this experiment via a custom web application (JavaScript v.1.7) that was hosted locally, allowing the observers to conduct the study through a web browser (Google chrome v.95.0.4638.54).

The second observer study used the visual grading characteristic (VGC) method [21] to compare the rankings of image quality at the preferred VMI energy level from the first observer study to the Mix and Threshold-1 images for each anatomic location. A five-point rating system ranging from excellent to poor (Table 1) was used to determine observers' image criteria scores. The two neuroradiologists participated in the second study.

Statistical and Visual Grading Analysis

Because our analysis was an exploratory study using the initial cohort, patient sample size was not determined prospectively.

Mean and standard deviation ROI measurements of image signal, noise, and SNR were reported across all patients. Shrout-Fleiss intraclass correlation coefficient was used to assess agreement between the four readers for their preference of VMIs at different energies in the first observer study. To analyze the observer image criteria scores from the VGC study, frequency tables were constructed to perform pairwise comparisons between VMI, Mix, and Threshold-1 images. The results from pairwise comparison between the Mix and Threshold-1 were not included.

Cumulative image criteria scores were plotted and the integral of each VGC curve (area under the curve, AUC_{VGC}) was used to display the difference in the image criteria scores between VMI and each of the two alternative image series, in a manner similar to receiver operating characteristic (ROC) analysis which plots cumulative diagnostic performance as decision threshold is varied. R statistical software (version 4.1.0; R Studio: Integrated Development Environment for R, Boston, MA) was used for all statistical analysis.

Results:

The final study population consisted of 15 subjects (mean age, 57 years; range, 46–75 years), including 7 men (mean age, 56 years; range, 46–72 years) and 8 women (mean age, 59 years; range, 48–75 years).

Quantitative analysis

Measurements of vasculature and CSF showed overall higher image noise compared to either grey or white matter. Decrease in noise as a function of keV was linear up to approximately 120 keV for vasculature and CSF and approximately 95 keV for white and grey matter and then plateaued. Threshold-1 had the lowest and Bin2 the highest noise for gray and white matter while vasculature and CSF images showed varying performance. At all anatomical locations, VMIs of 80 keV and above had lower noise than all binned or full spectral Threshold-1 images.

For each ROI, the highest SNR value was observed within a VMI rather than Mix, Bin1, Bin2, or Threshold-1 images across all patients. The energy level of the VMI that yielded the highest mean SNR value also varied by anatomical region with highest values in vascular structures. The highest SNR values for pons and midbrain were recorded at 65 keV, cisterna magna and medulla oblongata at 40 keV, common carotid, thalamus, and white matter at 70 keV, and internal jugular vein at 75 keV. Threshold-1 images had the highest mean SNR

across all anatomical regions except the cisterna magna where Bin1 had a higher SNR. Bin2 had the lowest mean SNR for all anatomical locations (Fig 1).

Qualitative Assessment

Figure 2 illustrates VMIs from 45–90 keV for a single subject at a single anatomic location. In the first observer study, there was high inter-reader agreement among the four readers on preferred VMI, with mean κ score of 0.89 (Fig 3). VMI energy levels of 50, 55, and 60 keV were preferred most frequently by observers accounting for 72% and 66% of preference ranks for carotid and jugular respectively. 50 keV was the highest ranked VMI for both vascular locations. For all other anatomic sites, 75, 80, and 85 keV were the most preferred VMIs. In the brainstem, these VMIs were preferred 66%, 64% and 68% for the pons, mid-brain, and medulla respectively. For the white matter and CSF, these VMIs were preferred for 67% and 78% respectively. VMIs at 80 keV was most frequently preferred for all non-vascular anatomical locations except the mid-brain where 85 keV was preferred.

In the second observer study using the VGC method, both readers ranked VMIs at the preferred energy level for each location higher in diagnostic quality than Mix and Threshold-1 images (Table 2). The two readers' AUC_{VGC} averaged over all anatomical locations were 0.67 and 0.72 for comparison to Mix images and 0.68 and 0.76 for comparison to Threshold-1 images. Both readers also ranked the VMI images higher than Mix and Threshold-1 images for vascular, grey matter, and white matter structures, and CSF. Representative images at the level of the brainstem are shown in Figure 4. Plots of cumulative image criteria scores for each observer at each confidence level comparing VMI to Mix and Threshold-1 images for each anatomic location are shown (Fig 5). The VGC curves can be interpreted as the reader's evaluation of diagnostic image quality of VMIs relative to either Mix or Threshold 1 images.

Discussion:

In PCCT of the head and neck, quantitative analysis of signal to noise measurements by location and by image reconstruction method demonstrated expected results. VMI images produced higher SNR values for each location compared to the polychromatic images. VMI's peak SNRs varied between the anatomic structure or tissues. The observer studies showed readers' preferred VMI energy level also varied by anatomic location and that observers rated the quality of VMIs higher than both the Mix and Threshold-1 images.

Our study agreed with findings in other qualitative studies of VMI in the head and neck using DECT. In our contrast enhanced study of the head and neck, VMIs were generated using the Mono+ algorithm (Siemens Healthineers). Grant et al developed and tested this technique which they describe as a regional spatial frequency-based recombination of the high signal present at lower energy and the superior noise characteristics at medium energy which are combined to avoid the increase in noise at low keV VMI [22]. In our study, the low-energy VMIs obtained from PCCT were shown to be preferred compared to Mix and Threshold-1 images, similar to findings of Albrecht et al who used the Mono+ VMI algorithm with contrast enhanced DECT of the head and neck compared to linear blended images [23]. Our study showed highest SNR in low energy VMIs and reader preferences

for 50–60 keV VMI for the carotid artery and jugular vein. This was slightly lower than the results of Schneider et al who found 60 keV VMI to be optimal for DECT angiography of the head and neck, implying an additional advantage of the Mono+ technique for optimizing low energy VMI [24].

Recently, an image quality assessment of PCCT angiography of the head and neck using the NAEOTOM Alpha scanner reported higher radiologist's quality ratings for polyenergetic images than for monoenergetic images for extra and intracranial arteries and cerebral arteries [25]. The difference between these results and our findings may be due to differences between our study aims and how the entire set of quality measures was reported. In our study, the VGC quality ratings for VMI for large vascular structures (Fig 5) were only slightly superior to polyenergetic images consistent with the report by Michael et al. However, we aimed to characterize brain tissues as well as vascular structures and report overall vascular and brain tissue quality for VMI versus polyenergetic imaging.

Our work presents readers' VMI preferences in a more complete graphical display than other image quality analyses of PCCT, utilizing an informative ROC-like graphical approach to compare image quality using reader studies. The display demonstrates that individual reader preferences vary by both location and keV level and that patterns vary between readers. This information is less apparent when agreement in reader preference is presented as a kappa statistic. These interesting data are typically lost due to averaging of the rankings and presentation in a tabular format and as has been done in comparable DECT work using Mono+ [23].

Our findings demonstrated that observers rated VMI overall higher in quality than the other methods of display and preferred levels for vascular evaluation at lower energies and brain tissues at higher energies. However, there was no single VMI energy that all observers preferred for all anatomic locations or clinical tasks. Based on these findings, we suggest that reconstructing a single VMI may not be sufficient for maximizing the technology's value across anatomic sites in a single exam and to reach full acceptance by the population of readers. In the future, reconstruction of a set of VMI energy levels may optimize interpretation of the anatomic structures and pathology within the PCCT scan but would require PACS viewing and workflow optimization.

Our study was performed on asymptomatic patients without major pathology and was performed as a CT angiogram, such that we could not evaluate the performance of VMI for tumor contrast enhancement, an important task in clinical CT of the head and neck. Images in this study were reconstructed using filtered back projection rather than iterative reconstruction as it was not yet available for the PCCT subsystem. Recently, the NAEOTOM Alpha scanner was released with iterative reconstruction optimized for spectral CT data (Quantum IR, Siemens) [26, 27]. We expect that the VMI images in our study had higher noise levels than would be seen if using the newer software. The image quality ratings for VMI would likely have been even higher and VGC curves would likely have shown a greater degree of superiority of VMI compared to Threshold-1 and Mix images. We also did not explore optimization of image display window width and level for determining preferred VMI energy level. Observers were presented with standard, fixed, image display values

which may have resulted in bias towards an image appearance comparable to conventional EID image appearance at standard display values. Fu et al have shown it is likely that optimal adjustments of window values may result in higher image quality ratings and preferences for lower keV VMI images [28].

In conclusion, our study demonstrated superior image quality ratings using Monoplus-generated VMI compared to mixed and polychromatic images. Based on our findings of reader preferences, workflow optimization such as additional VMIs at a variety of energy levels displayed according to anatomic location or task may ultimately prove to be useful rather than one workflow-fits-all approach.

Funding:

Please use: This study was supported by the National Institutes of Health (NIH) Clinical Center Radiology and Imaging Sciences (RADIS), the NIH Graduate Partnership Program and the NIH Intramural Research Program.

Declaration of Interest

This study was supported by the National Institutes of Health (NIH) Clinical Center Radiology and Imaging Sciences (RADIS), the NIH Graduate Partnership Program and the NIH Intramural Research Program. The NIH and Siemens Medical Solutions have a Cooperative Research and Development Agreement providing material support, including the photon-counting CT system. Co-authors Pooyan Sahbaee, PhD, Ralf Gutjahr, PhD, and Thomas G. Flohr, PhD are employees of Siemens. NIH co-authors had final control over the data analysis and content of the manuscript.

This work originated at:

Radiology and Imaging Sciences, Clinical Center, National Institutes of Health (NIH), 10 Center Drive, Bethesda, MD 20892

References

[1]. Hounsfield GN. Computerized transverse axial scanning (tomography). 1. Description of system. Br J Radiol 1973;46(552):1016–22. [PubMed: 4757352]

[2]. Alvarez RE, Macovski A. Energy-selective reconstructions in X-ray computerized tomography. Phys Med Biol 1976;21(5):733–44. [PubMed: 967922]

[3]. Leng S, Yu L, Wang J, Fletcher JG, Mistretta CA, McCollough CH. Noise reduction in spectral CT: reducing dose and breaking the trade-off between image noise and energy bin selection. Med Phys 2011;38(9):4946–57. [PubMed: 21978039]

[4]. Yu L, Primak AN, Liu X, McCollough CH. Image quality optimization and evaluation of linearly mixed images in dual-source, dual-energy CT. Med Phys 2009;36(3):1019–24. [PubMed: 19378762]

[5]. Yu L, Christner JA, Leng S, Wang J, Fletcher JG, McCollough CH. Virtual monochromatic imaging in dual-source dual-energy CT: radiation dose and image quality. Med Phys 2011;38(12):6371–9. [PubMed: 22149820]

[6]. Danielsson M, Persson M, Sjolin M. Photon-counting x-ray detectors for CT. Phys Med Biol 2021;66(3):03TR1.

[7]. Taguchi K. Energy-sensitive photon counting detector-based X-ray computed tomography. Radiol Phys Technol 2017;10(1):8–22. [PubMed: 28138947]

[8]. Ballabriga R, Alozy J, Bandi FN, Campbell M, Egidos N, Fernandez-Tenllado JM, et al. Photon Counting Detectors for X-Ray Imaging With Emphasis on CT. IEEE Trans Radiat Plasma Med Sci 2021;5(4):422–40.

[9]. Pourmorteza A, Symons R, Sandfort V, Mallek M, Fuld MK, Henderson G, et al. Abdominal Imaging with Contrast-enhanced Photon-counting CT: First Human Experience. Radiology 2016;279(1):239–45. [PubMed: 26840654]

[10]. Symons R, Pourmorteza A, Sandfort V, Ahlman MA, Cropper T, Mallek M, et al. Feasibility of Dose-reduced Chest CT with Photon-counting Detectors: Initial Results in Humans. Radiology 2017;285(3):980–9. [PubMed: 28753389]

[11]. Symons R, Cork TE, Sahbaee P, Fuld MK, Kappler S, Folio LR, et al. Low-dose lung cancer screening with photon-counting CT: a feasibility study. Phys Med Biol 2017;62(1):202–13. [PubMed: 27991453]

[12]. Pourmorteza A, Symons R, Reich DS, Bagheri M, Cork TE, Kappler S, et al. Photon-Counting CT of the Brain: In Vivo Human Results and Image-Quality Assessment. AJNR Am J Neuroradiol 2017;38(12):2257–63. [PubMed: 28982793]

[13]. Symons R, Reich DS, Bagheri M, Cork TE, Krauss B, Ulzheimer S, et al. Photon-Counting Computed Tomography for Vascular Imaging of the Head and Neck: First In Vivo Human Results. Invest Radiol 2018;53(3):135–42. [PubMed: 28926370]

[14]. Ferda J, Vendis T, Flohr T, Schmidt B, Henning A, Ulzheimer S, et al. Computed tomography with a full FOV photon-counting detector in a clinical setting, the first experience. Eur J Radiol 2021;137:109614.

[15]. Euler A, Higashigaito K, Mergen V, Sartoretti T, Zanini B, Schmidt B, et al. High-Pitch Photon-Counting Detector Computed Tomography Angiography of the Aorta: Intraindividual Comparison to Energy-Integrating Detector Computed Tomography at Equal Radiation Dose. Invest Radiol 2022;57(2):115–21. [PubMed: 34352805]

[16]. Sartoretti T, Mergen V, Higashigaito K, Eberhard M, Alkadhi H, Euler A. Virtual Noncontrast Imaging of the Liver Using Photon-Counting Detector Computed Tomography: A Systematic Phantom and Patient Study. Invest Radiol 2022;57(7):488–93. [PubMed: 35136003]

[17]. Allmendinger T, Nowak T, Flohr T, Klotz E, Hagenauer J, Alkadhi H, et al. Photon-Counting Detector CT-Based Vascular Calcium Removal Algorithm: Assessment Using a Cardiac Motion Phantom. Invest Radiol 2022;57(6):399–405. [PubMed: 35025834]

[18]. FDA Clears First Major Imaging Device Advancement for Computed Tomography in Nearly a Decade, https://www.fda.gov/news-events/press-announcements/fda-clears-first-major-imaging-device-advancement-computed-tomography-nearly-decade; September 30, 2021 Accessed November 12, 2021.

[19]. Rajendran K, Petersilka M, Henning A, Shanblatt ER, Schmidt B, Flohr TG, et al. First Clinical Photon-counting Detector CT System: Technical Evaluation. Radiology 2022;303(1):130–8. [PubMed: 34904876]

[20]. Yu Z, Leng S, Jorgensen SM, Li Z, Gutjahr R, Chen B, et al. Evaluation of conventional imaging performance in a research whole-body CT system with a photon-counting detector array. Phys Med Biol 2016;61(4):1572–95. [PubMed: 26835839]

[21]. Bath M, Mansson LG. Visual grading characteristics (VGC) analysis: a non-parametric rank-invariant statistical method for image quality evaluation. Br J Radiol 2007;80(951):169–76. [PubMed: 16854962]

[22]. Grant KL, Flohr TG, Krauss B, Sedlmair M, Thomas C, Schmidt B. Assessment of an advanced image-based technique to calculate virtual monoenergetic computed tomographic images from a dual-energy examination to improve contrast-to-noise ratio in examinations using iodinated contrast media. Invest Radiol 2014;49(9):586–92. [PubMed: 24710203]

[23]. Albrecht MH, Scholtz JE, Kraft J, Bauer RW, Kaup M, Dewes P, et al. Assessment of an Advanced Monoenergetic Reconstruction Technique in Dual-Energy Computed Tomography of Head and Neck Cancer. Eur Radiol 2015;25(8):2493–501. [PubMed: 25680727]

[24]. Schneider D, Apfaltrer P, Sudarski S, Nance JW Jr., Haubenreisser H, Fink C, et al. Optimization of kiloelectron volt settings in cerebral and cervical dual-energy CT angiography determined with virtual monoenergetic imaging. Acad Radiol 2014;21(4):431–6. [PubMed: 24594412]

[25]. Michael AE, Boriesosdick J, Schoenbeck D, Lopez-Schmidt I, Kroeger JR, Moenninghoff C, et al. Photon Counting CT Angiography of the Head and Neck: Image Quality Assessment of Polyenergetic and Virtual Monoenergetic Reconstructions. Diagnostics (Basel) 2022;12(6).

[26]. Higashigaito K, Euler A, Eberhard M, Flohr TG, Schmidt B, Alkadhi H. Contrast-Enhanced Abdominal CT with Clinical Photon-Counting Detector CT: Assessment of Image Quality and

Comparison with Energy-Integrating Detector CT. Acad Radiol 2022;29(5):689–97. [PubMed: 34389259]

[27]. Sartoretti T, Landsmann A, Nakhostin D, Eberhard M, Roeren C, Mergen V, et al. Quantum Iterative Reconstruction for Abdominal Photon-counting Detector CT Improves Image Quality. Radiology 2022;303(2):339–48. [PubMed: 35103540]

[28]. Fu W, Marin D, Ramirez-Giraldo JC, Choudhury KR, Solomon J, Schabel C, et al. Optimizing window settings for improved presentation of virtual monoenergetic images in dual-energy computed tomography. Med Phys 2017;44(11):5686–96. [PubMed: 28777467]

Highlights

1. Peak SNR was between VMI energies of 45–75 keV for all anatomic locations representing diagnostic imaging tasks.
2. Radiologists preferred a VMI range of 50–60 keV for vascular tasks and 75–85 keV for cerebrospinal fluid, and the low contrast soft tissue discriminatory tasks in brain.
3. In a comparison of image quality ratings, both readers preferred virtual monoenergetic images over linear mix of low and high energies and full spectrum images.

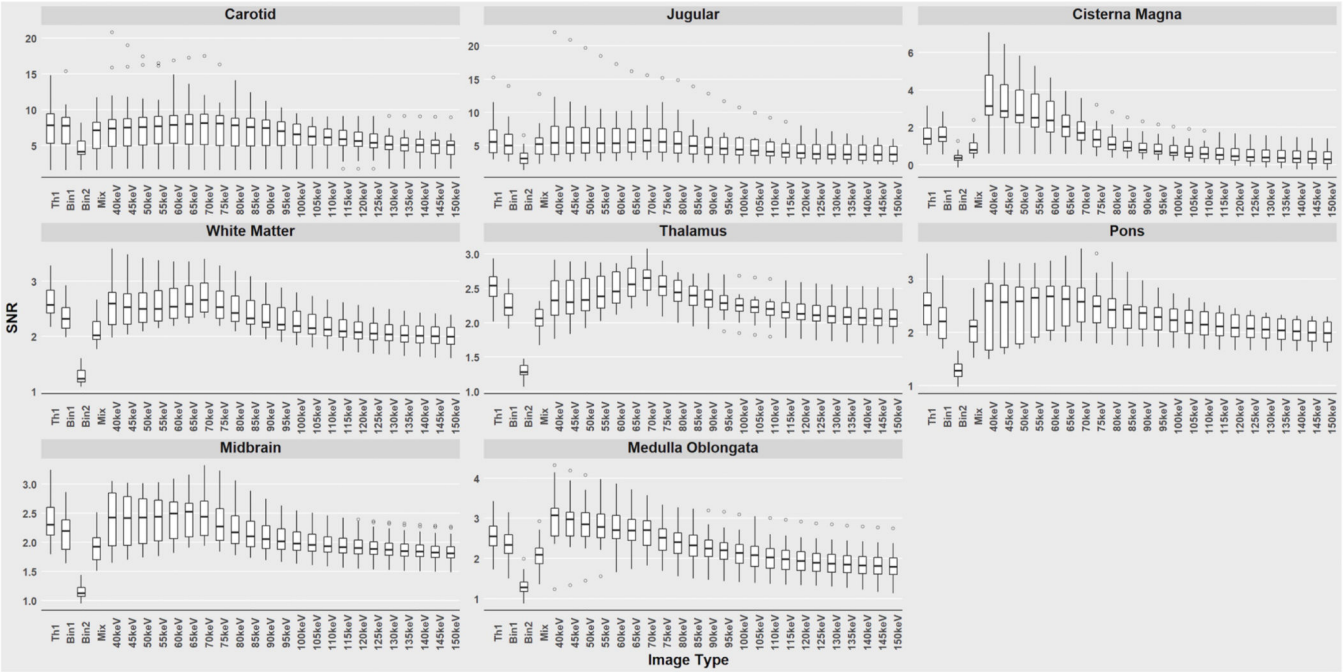

Figure 1:

Signal-to-noise ratios (SNR) for all images calculated from regions of interest at different anatomical locations. Boxplots are shown with conventional polychromatic sets (Threshold-1 (Th1), Bin1, Bin2, Mix) at the left side of the x-axis and virtual monoenergetic image sets (40–150 keV) on the right. Note that the SNR scale varies among the graphs. Outlier values are represented by dots separated from the main boxplot.

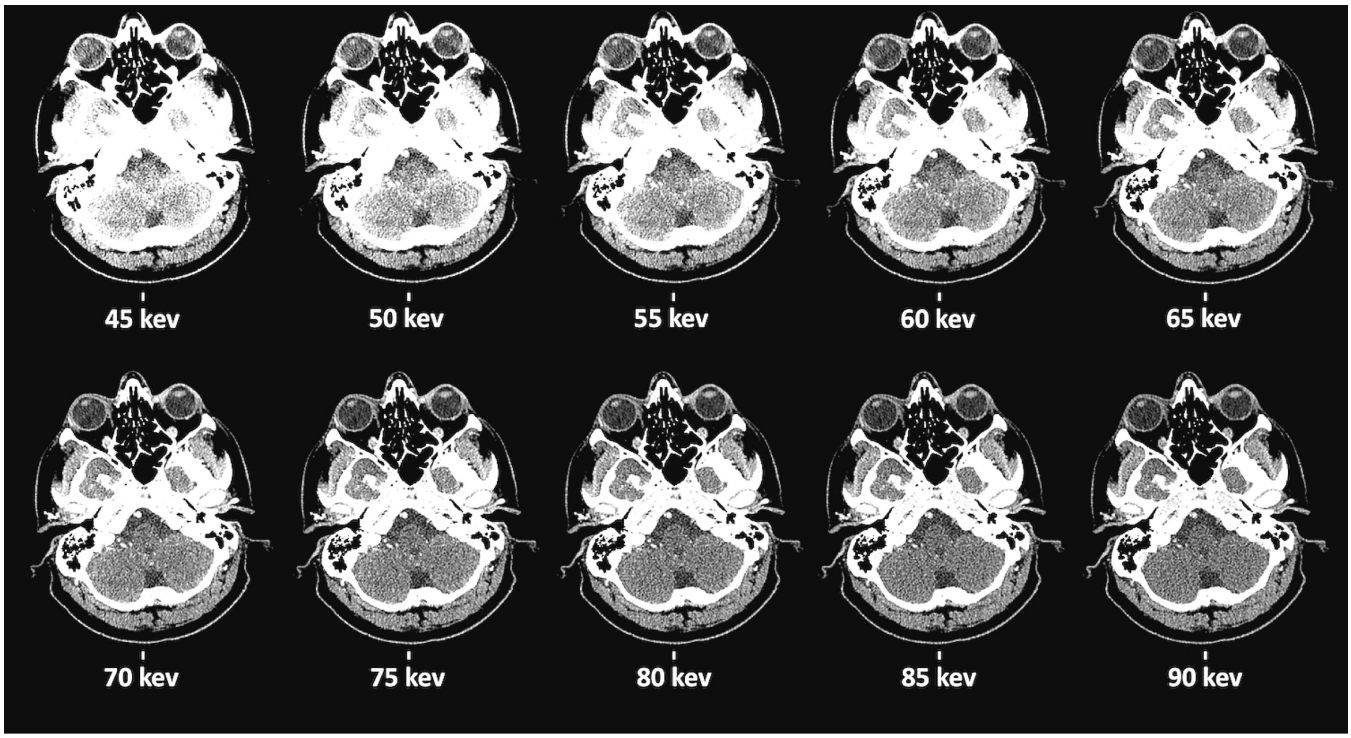

Figure 2:

Axial virtual monoenergetic images (VMI) of the cisterna magna in the range 45–90 keV for one patient. A sample task, cisterna magna, reviewed by radiologists as part of the observer study to indicate preference of VMI energy levels at various anatomical sites. For this figure, images are sorted by increasing monochromatic energy level.

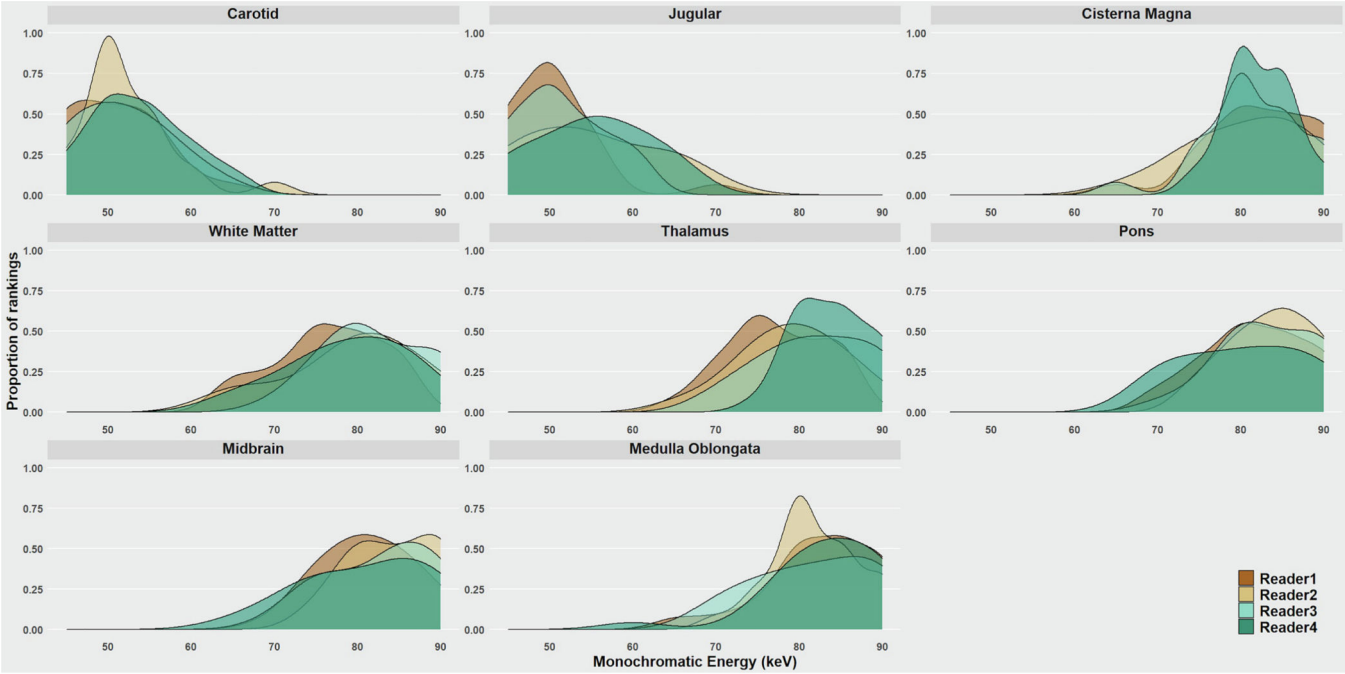

Figure 3:

Observer study to determine the preferred virtual monoenergetic image (VMI) energy level at each anatomical location. Distribution of radiologist preference ratings plotted against VMI energy levels. Excellent reader consistency was shown across all readers. Optimal VMI for vascular structures was 40–60 keV and for soft tissues 80–90 keV.

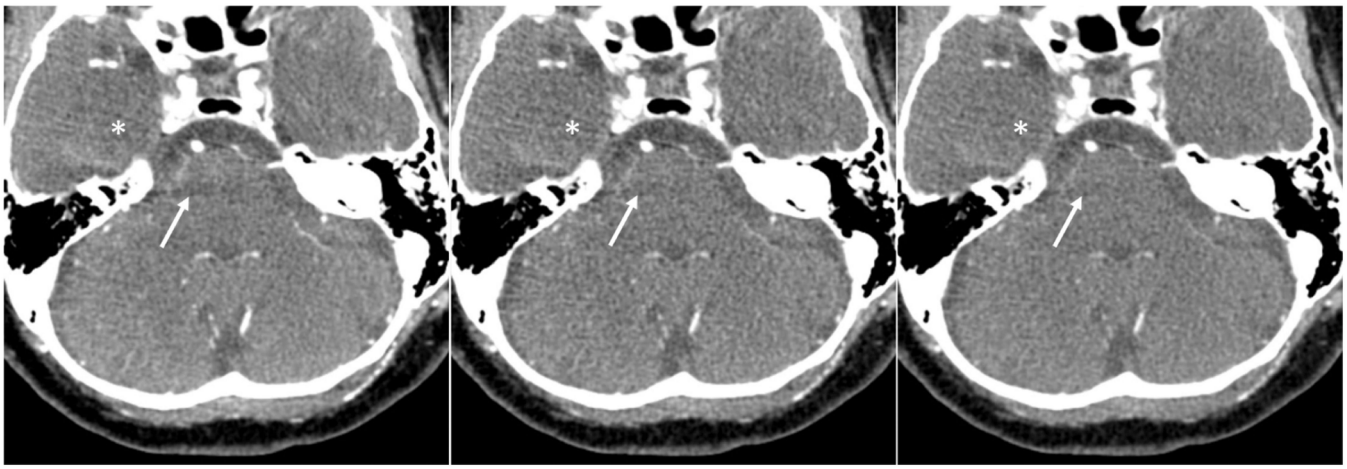

Figure 4:

Contrast enhanced photon-counting CT scan of a 58-years-old male with different reconstructions. Axial images of brain including the posterior fossa were reconstructed as Threshold 1 (25–140 keV) (left panel), Mix (0.6 Bin1:0.4 Bin2 ratio) (middle panel), and 80 keV virtual monoenergetic (right panel) images. Beam hardening artifact in the posterior fossa (arrows) reduced the visibility of brainstem structures. In the virtual monoenergetic images, beam hardening artifact and noise (asterisk) are reduced.

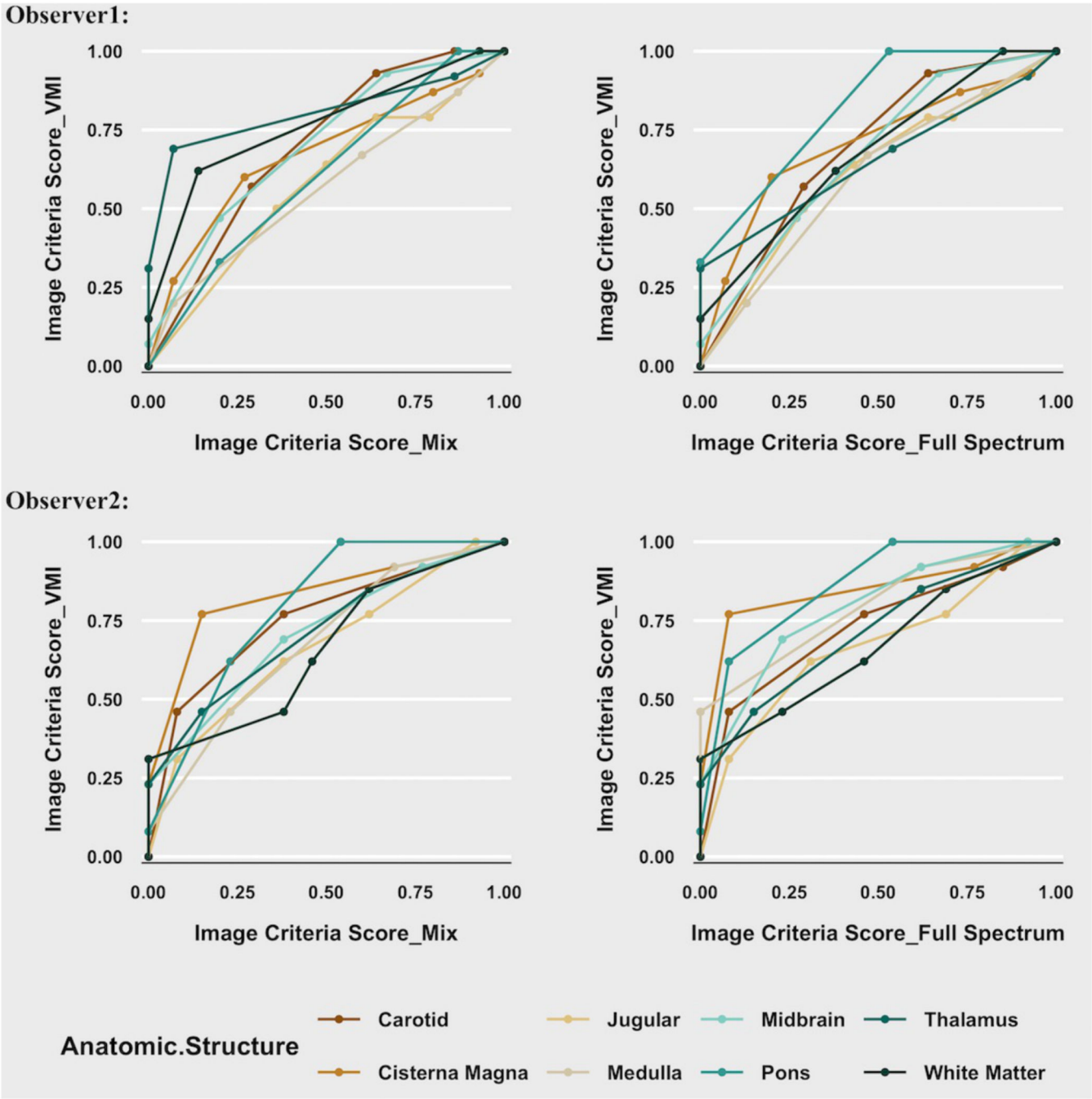

Figure 5:

Visual grading characteristic (VGC) curves for the image criteria scores comparing Mix and Threshold-1 images for each anatomic location. The image criteria scores (ICS) cumulative values of observers' confidence that the image is of diagnostic quality in the virtual monoenergetic images (VMI) are plotted against those of the mixed images (Mix) (left column) and full-spectrum threshold-1 (Th1) (right column) for observer 1 (top row) and observer 2 (bottom row). The circles represent the coordinates corresponding to the observers' categorization of images based on the ordinal rating scale. As in receiver

operating characteristic analysis, a curve shifted to the left upper corner indicates higher quality for the image set plotted on Y axis. A diagonal plot (line of equality) would imply observer ratings were equivalent between the 2-image series.

Table 1.

Image criteria score used in the visual grading characteristic study.

Image criteria score	Description
1-excellent	No limitations for clinical use.
2-good	Minimal limitations for clinical use.
3-sufficient	Moderate limitations for clinical use but no substantial loss of information.
4-restricted	Relevant limitations for clinical use, clear loss of information.
5-poor	Image not usable, loss of information, image must be repeated.

Table 2.

Area under the curve (AUC_{VGC}) for the visual grading characteristic (VGC) study. The AUC_{VGC} for VMI compared to the linearly blended (Mix) and full spectrum (Threshold-1) images are shown for both readers for each anatomic location.

Location	VMI vs Mix (Reader 1, Reader 2)	VMI vs Threshold-1 (Reader 1, Reader 2)
Averaged over all locations	0.67, 0.72	0.68, 0.76
Vascular	0.64, 0.71	0.65, 0.70
Grey matter	0.67, 0.72	0.69, 0.79
White matter	0.76, 0.66	0.68, 0.67
Cerebrospinal fluid	0.67, 0.83	0.70, 0.85